Terra and Aqua MODIS TEB intercomparison using Himawari-8/AHI as reference

Tiejun Chang
Xiaoxiong Xiong
Amit Angal

SPIE.

Terra and Aqua MODIS TEB intercomparison using Himawari-8/AHI as reference

Tiejun Chang,[a,]* Xiaoxiong Xiong,[b] and Amit Angal[a]

[a]Science Systems and Applications, Inc., Lanham, Maryland, United States
[b]Sciences and Exploration Directorate, NASA/GSFC, Greenbelt, Maryland, United States

Abstract. Intercomparison between the two MODIS instruments is very useful for both the instrument calibration and its uncertainty assessment. Terra and Aqua MODIS have almost identical relative spectral response, spatial resolution, and dynamic range for each band, so the site-dependent effect from spectral mismatch for their comparison is negligible. Major challenges in cross-sensor comparison of instruments on different satellites include differences in observation time and view angle over selected pseudoinvariant sites. The simultaneous nadir overpasses (SNO) between the two satellites are mostly applied for comparison and the scene under SNO varies. However, there is a dearth of SNO between the Terra and Aqua. This work focuses on an intercomparison method for MODIS thermal emissive bands using Himawari-8 Advanced Himawari Imager (AHI) as a reference. Eleven thermal emissive bands on MODIS are at least to some degree spectrally matched to the AHI bands. The sites selected for the comparison are an ocean area around the Himawari-8 suborbital point and the Strzelecki Desert located south of the Himawari-8 suborbital point. The time difference between the measurements from AHI and MODIS is <5 min. The comparison is performed using 2017 collection 6.1 L1B data for MODIS. The MODIS–AHI difference is corrected to remove the view angle dependence. The Terra–Aqua MODIS difference for the selected TEB is up to 0.6 K with the exception of band 30. Band 30 has the largest difference, which is site dependent, most likely due to a crosstalk effect. Over the ocean, the band 30 difference between the two MODIS instruments is around 1.75 K, while over the desert; the difference is around 0.68 K. The MODIS precision is also compared from the Gaussian regression of the double difference. Terra bands 27 to 30 have significant extra noise due to crosstalk effects on these bands. These Terra–Aqua comparison results are used for MODIS calibration assessments and are beneficial for future calibration algorithm improvement. The impact of daytime measurements and the scene dependence are also discussed. © *2019 Society of Photo-Optical Instrumentation Engineers (SPIE)* [DOI: 10.1117/1.JRS.13.017501]

Keywords: intercomparison; MODIS; TEB; radiometric calibration; Himawari-8; AHI.

1 Introduction

The Moderate Resolution Imaging Spectroradiometer (MODIS) instruments on-board the Terra and Aqua satellites have successfully operated since their launch in 1999 and in 2002, providing more than 18 and 16 years of continuous global observations, respectively.[1,2] Over a decade of continuous global observations have produced an unprecedented amount of science data products monitoring land surface temperature, sea surface temperature, cloud top altitude and temperature, and water vapor content.[3–11]

The two MODIS instruments use similar on-board calibrators and on-orbit calibration algorithms. The instrument calibration and uncertainty assessment are very useful for the calibration improvement and their product consistency. The near-identical relative spectral response, spatial resolution, and dynamic range for each band provide advantages for the comparison. The uncertainties associated with site-specific corrections for a mismatch in these parameters are

---

*Address all correspondence to Tiejun Chang, E-mail: tiejun.chang@ssaihq.com

significantly reduced. However, Terra is in the morning orbit with an equator crossing time of 10:30 am, and Aqua is in the afternoon orbit with equator crossing time of 1:30 pm. Due to the lack of simultaneous nadir overpasses (SNO) between the two MODIS instruments, the intercomparison of the thermal emissive bands (TEB) is particularly challenging. To achieve a high precision intercomparison between instruments with different observation times is particularly challenging for the TEB. In this work, the intercomparisons of MODIS thermal bands are performed over selected ground targets, using the observations from a sensor on-board a geostationary (GEO) satellite as a bridge. The double difference method is applied to assess the brightness temperature (BT) measurements between the two MODIS instruments using the geostationary imager. Himawari-8 was launched on October 7, 2014. The Advanced Himawari Imager (AHI) on-board the Himawari-8 satellite is used as a reference for the comparing Terra and Aqua MODIS. AHI has 16 channels with spatial resolutions from 0.5 to 2 km at nadir and produces full disk observations every 10 min. Due to the full disk and near-continuous observations from AHI, many different types of scenes and sites can be analyzed for comparisons with various effects. Two comparisons presented in this paper include an ocean site at AHI nadir and a desert site in Australia. The MODIS collection 6.1 (C6.1) L1B data and AHI L1B data are used. The comparison results will be helpful as an assessment of the consistency in the TEB calibration of the MODIS instruments and the possibility of future enhancements to the L1B product.

The intersatellite sensor comparisons for thermal bands have been performed for MODIS. Xiong et al. and Chander et al have published overviews on the methods for the sensor intercomparisons.[12,13] The methods applied to MODIS TEB include the use of satellite observations from SNO and the use of the ground targets as Refs. [14–22]. The performance and calibration accuracy are assessed using difference between sensors, double difference using an independent reference, and the long-term trending of the comparison.[12,13] The ground targets most often used include Dome Concordia (Dome C) site in Antarctica, Lake Tahoe, ocean buoys, and various land sites. Ground measurements have also been used as references. The SNO method has been widely used for intercomparison of both solar reflective and TEB. The Infrared Atmospheric Sounding Interferometer (IASI) on MetOp-A and MetOp-B and the Atmospheric Infrared Sounder (AIRS) on Aqua are used to assess MODIS TEB performance based on the long-term trending. The SNO for two low earth orbit (LEO) satellites are limited by the quantity of comparison samples and scene availability.

The intercomparison over a large BT range and various scene types can be very useful in assessing the instrument calibration and uncertainty. As a result, the uncertainties associated with mismatch in site-specific corrections are significantly reduced. However, using ground measurements as a reference, such as Dome C, can only provide comparisons covering low BTs over ice and snow scenes. As Terra is a morning satellite and Aqua is an afternoon satellite, the time difference between the two measurements and the reference also introduces additional uncertainty in the comparison.

In this work, measurements from a GEO sensor are used as a near-simultaneous reference over selected scenes. For example, as AHI on Himawari-8 provides a full disk image every 10 min and the observation time difference between MODIS and AHI is <5 min. Various scenes are available for selection and cover a wide range of BT. For a given scene, the impact of observation time, spectral, and view angle differences are reduced using physical model, empirical model, or typical measurement over the selected scene. In addition, this method provides an enormous number of samples that further reduce the comparison uncertainty. The degree of spectral band matching, comparable spatial resolution, and near-simultaneous observations make the double difference method feasible for comparing the two MODIS instruments. By using clear sky measurements, this comparison method minimizes the impact of the difference in observation time for scenes with similar viewing conditions. Section 2.1 reviews the methodology for MODIS TEB intercomparison between satellite sensors. Section 2.2 presents the background of MODIS and AHI instruments as well as their spectral band matching. Section 3 presents the methodologies applied in this work, including site selection, data resampling, cloud filtering, corrections, and double difference. Section 4 presents the comparison results and Sec. 5 discusses the results of the comparison.

2 Instrument Overview

2.1 MODIS

MODIS has 16 TEB, covering the midwave infrared (MWIR: bands 20 to 25) and long-wave infrared (LWIR: bands 27 to 36) spectral regions. All TEB are located on two cold focal plane assemblies (CFPAs): a short-wave and midwave infrared (SMIR) FPA and an LWIR FPA. The CFPAs are nominally controlled on-orbit at 83 K using a passive radiative cooler. Bands 20 to 25 and 27 to 30 consist of 10 photovoltaic (PV) detectors per band, while bands 31 to 36 consist of 10 photoconductive detectors per band. The on-board BB serves as the primary calibration source and the space view provides a reference for the instrument background and offsets. The BB temperature is measured using a set of 12 thermistors. For nominal operations, the BB temperature is set at 290 K for Terra MODIS and 285 K for Aqua MODIS. MODIS TEB calibration uses a quadratic calibration algorithm on a scan-by-scan basis for each TEB detector. [1,23] During the BB WUCD cycles, the BB temperature varies from instrument ambient (∼270 K) to 315 K. The BB WUCD is used to characterize the on-orbit change in the instrument's nonlinear response coefficients. The linear coefficient of the response function for each TEB is calibrated scan-by-scan with the nonlinear coefficient and offset from an offline lookup table (LUT) derived from the quarterly WUCD events.

Terra and Aqua MODIS C6.1 L1B has significant improvements compared to previous collections.[1] One of the major improvements is the reduction of the electronic crosstalk effect. As the mission has progressed, the effects of electronic crosstalk among the Terra MODIS PV-LWIR bands 27 to 30 have become increasingly large and its impact on L1B products has grown.[24] To characterize and correct the signal contamination from electronic crosstalk, Moon observations have been used to derive the appropriate correction coefficients, which are applied to the detector's digital response data for Terra MODIS bands 27 to 30. The correction has been implemented in C6.1 over the entire mission and is being continuously monitored and updated in the forward production.

2.2 AHI

The Himawari-8 spacecraft was launched on October 7, 2014 at an altitude of ∼35,800 km, longitude of ∼140.7° east, covering the East Asia and Western Pacific regions. The primary instrument aboard Himawari-8, AHI, is a 16-channel multispectral imager that captures visible and infrared images of the Asia-Pacific region.[25] AHI has a very similar design and spectral channels as Advanced Baseline Imager (ABI) on-board US GOES-16. Both the instruments were designed and built by Harris Corporation (formerly ITT Exelis Geospatial Systems) and represent a significant improvement over the imager on-board previous GOES satellites.[26] AHI uses two scan mirrors (north-south and east-west scan mirrors) and produces a full disk observation every 10 min with a resolution down to 500 m.[27] The AHI instrument features higher spatial, spectral, and radiometric resolution than previous imagers on-board geostationary satellites, besides shortened scanning. It has 3 visible, 3 near-infrared, and 10 infrared bands. The spatial resolution is 2 km at nadir for TEB. The TEBs show a significant nonlinear response and hence a quadratic response function is used for the calibration.[28] The linear coefficient of the response function for each channel is calibrated every 10 min using an on-board BB with the nonlinear coefficients derived from prelaunch testing. Compared to previous imagers on-board geostationary satellites, AHI and ABI provide more spectral channels, higher spatial resolution, and enhanced radiometric calibration accuracy.

2.3 Spectral Matching Bands

The MODIS and AHI matching bands are listed in Table 1 and their RSR functions are shown in Fig. 1. The method used in this work is the double difference and AHI is used as a bridge to facilitate a comparison between Terra and Aqua MODIS. Hence, the effect of differences in spectral response function between MODIS and AHI is insignificant to the first order. However, for a specific site, the spectral mismatch can have an effect that varies seasonally

Table 1 The center wavelength for the matching bands of MODIS and AHI.

MODIS band	20	21	22	23	27	28	29	30	31	32	33
MODIS wavelength (μm)	3.78	3.97	3.97	4.05	6.77	7.34	8.53	9.73	11.02	12.03	13.36
AHI band			7			9	10	11	12	14	15	16
AHI wavelength (μm)			3.88			6.94	7.35	8.59	9.64	11.24	12.38	13.28
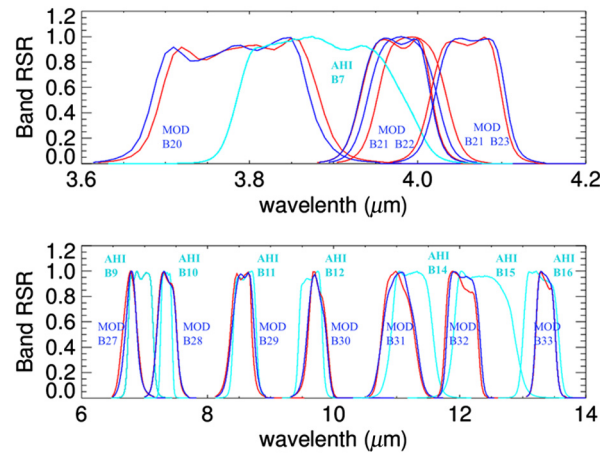
Fig. 1 The spectral response function of the selected bands of MODIS (Terra in blue and Aqua in red) and AHI (light blue).

or with observation time. The analysis in this work uses the averaged results over the entire year to minimize this effect. For most of the matching bands, AHI bands have broader spectral response functions than MODIS. Four matching MODIS bands, 20 to 23, are compared with AHI band 7 centered at 3.9 μm.

The imperfect matching between AHI bands and MODIS bands can impact the comparison results between MODIS and AHI. As presented in Refs. 12 and 13, the double difference method, by using intermediate transfer instrument as a reference, can be used to compare MODIS and AVHRR, as well as LEO-GEO-LEO comparison.[12,13] To minimize the spectral mismatch impact, a selected type of stable and uniform scene should be used. In this work, uniform clear sky ocean and desert sites are selected for applying the double difference method, as presented in Sec. 3.1. The uniformity and cloud screening, presented in Sec. 3.2, are also necessary to ensure a stable reference for this double difference technique. The slight spectral difference between Terra MODIS and Aqua MODIS has insignificant impact on the comparison between Terra and Aqua MODIS. This effect is discussed in Sec. 5.1.

3 Methodology Development

3.1 Site Selection and Resampling

In this paper, an area of ocean located under AHI nadir and a site around the Strzelecki Desert to the south of AHI nadir have been selected.[29,30] The full disk of AHI does not cover the widely used North African desert sites, including Libya 4. The Strzelecki Desert in South Australia has been used previously as a bright calibration target.[29,30] When AHI views the site near its nadir, the zero angle of the AHI east-west scan mirror and small view angle may enhance its reference accuracy. The BT varies with time of a day and solar angle. The observation time difference also introduces uncertainty due to the presence of clouds and varying atmospheric conditions. Hence, the comparisons should be performed using simultaneous overpasses with minimal time

difference. MODIS images a given site in daytime and in nighttime once every 1 to 2 days. AHI images the Earth's full disk every 10 min. The higher temporal sampling of AHI makes it possible to shorten the overpass time difference between MODIS and AHI for the selected sites. For clear sky measurements, the effects of up to 5 min time difference can be averaged out and the impact on the comparison will be greatly reduced.

This work employs a pixel-to-pixel comparison between MODIS and AHI. However, the AHI pixel size at nadir is 2 km for the TEB and MODIS pixel size at nadir is 1 km for the TEB. The geolocation error and pixel mismatch should also be considered. The MODIS measurements with different view angles are used for comparison and a correction of the view angle dependence is necessary. Table 2 lists the geolocation of the site and MODIS overpass time (day and night).

The L1B data from MODIS C6.1 and AHI are processed for comparison. There are two methods for the comparison for the selected site. (1) Average all pixels within the enclosed region of interest and then perform a BT comparison and (2) resample the pixels within the enclosed region of interest from one of the instruments and then perform a pixel-to-pixel comparison. The first method is simpler, but may introduce additional uncertainties. It also causes issue for the area with small number of cloudy pixels. In this paper, a pixel-to-pixel comparison after resampling is used. The MODIS data are resampled and interpolated to the AHI grid over the selected area, as shown in Fig. 2. Even though scene uniformity was a major consideration in the site selection process, the presence of clouds can cause nonuniformity over the site. The pixel-to-pixel comparison after resampling enhances the comparison accuracy and also allows the comparison to be performed over a broad range of BTs.

Table 2 The latitude and longitude ranges (in degrees) of the calibration sites, AHI pixel number, MODIS overpass time, and overpass granule number used for comparison in year 2017.

| | | | | Passing time (UTC) | | | | Granule number | | | |
| | | | | Terra | | Aqua | | Terra–AHI | | Aqua–AHI | |
Site	Lat	Lon	AHI pixel number	Day	Night	Day	Night	Day	Night	Day	Night
AHI nadir (ocean)	−1.00 to 1.00	+139.70 to +140.70	100 × 100	00:10 to 01:50	12:20 to 14:00	03:20 to 05:00	15:10 to 16:50	521	492	497	530
Strzelecki desert	−30.5 to −28.5	+138.8 to +140.8	100 × 100	23:30 to 01:40	12:30 to 14:35	03:45 to 05:35	14:35 to 16:45	484	559	547	496

Himawari-8 AHI image   Aqua MODIS Image   Aqua MODIS resampled image
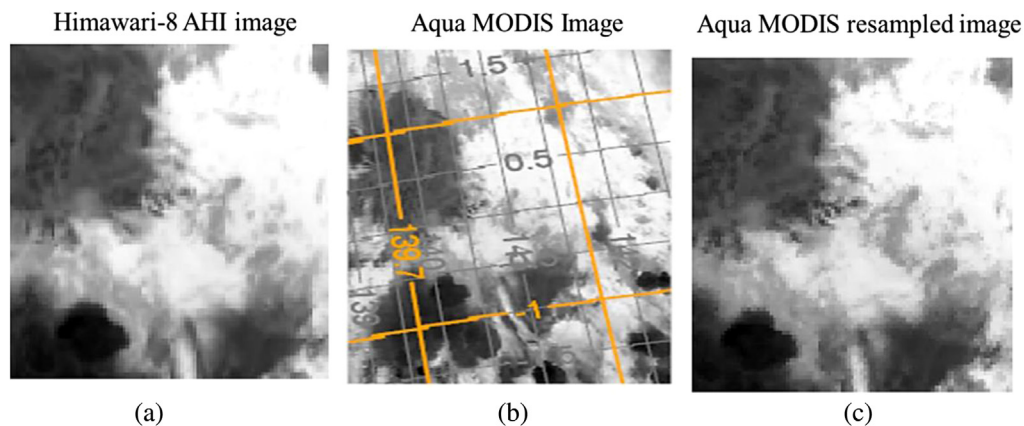
(a)   (b)   (c)

Fig. 2 (a) The AHI image of selected ocean site (granule time stamp 20171228_1550). (b) Aqua MODIS image covering the same site (granule time stamp 2017362.1550). The yellow lines are the latitude and longitude boundaries for the site. (c) Resampled Aqua MODIS image of the site with AHI grid.

3.2 *Uniformity and Cloud Screening*

As stated earlier, the spatial resolution for AHI TEB is 2 km while it is only 1 km for MODIS TEB. The data resampling and sensor spatial uncertainty reduce the comparison accuracy when using observations over a nonuniform scene. The observation time difference also has effects if there are clouds present or the atmospheric conditions change between the two overpasses. MODIS C6.1 level 2 products (MOD35 for Terra and MYD35 for Aqua) are used for identifying cloudy and clear sky measurements.[31] The cloud mask has four values indicating cloudy, partially cloudy, partially clear, and clear. The pixels selected for comparison are totally clear sky. The scene uniformity is assessed using the cloud mask of surrounding pixels. A pixel selected for comparison should have the same cloud mask status (clear) over the 3 × 3 resampled AHI pixels. Additional uniformity filtering is also applied by using the variation over nine (3 × 3) AHI pixels
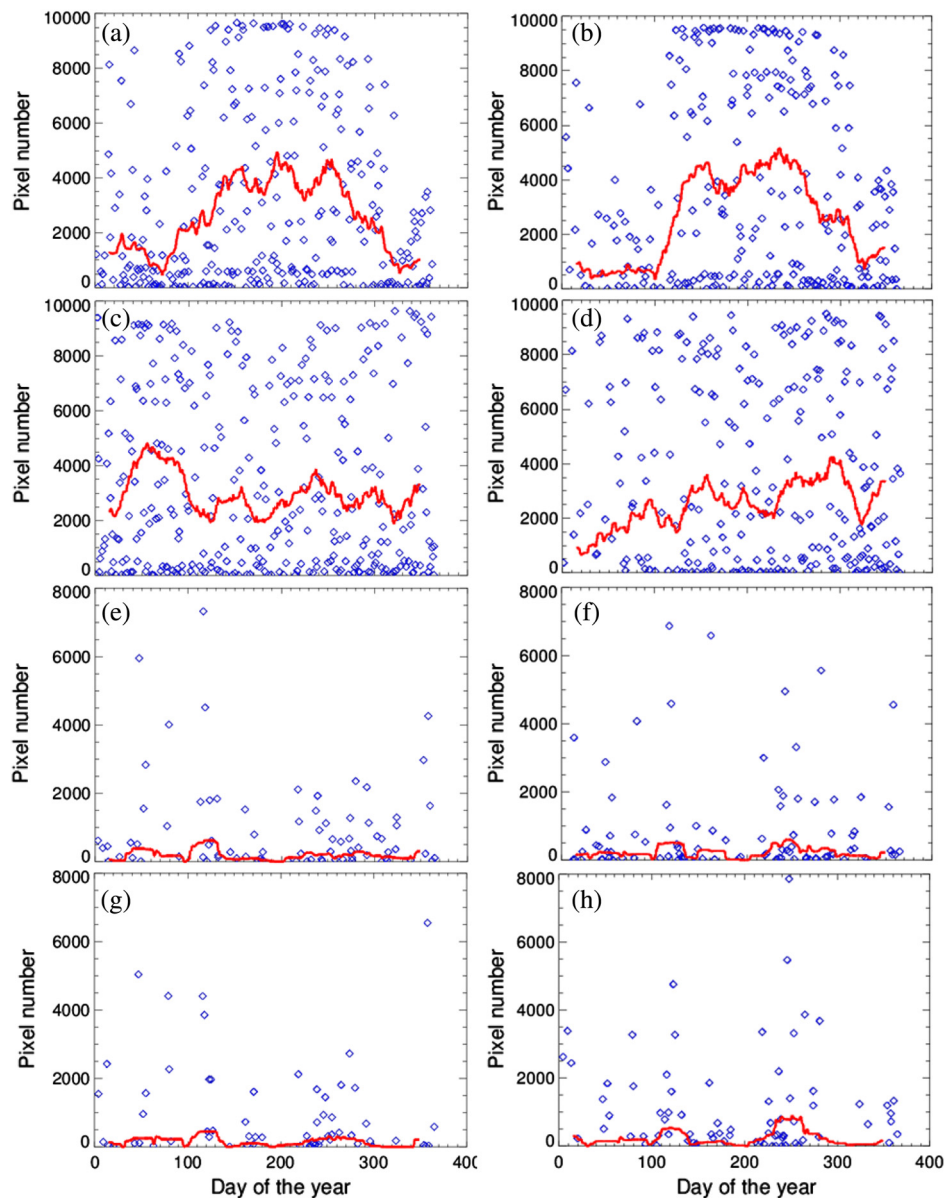

Fig. 3 The AHI pixel count for the selected sites after the uniformity and clear sky filtering. The blue symbols are the pixel number for a day of the year (2017) and the red lines are the 30-day moving average to show the seasonal trend. The left hand charts are for Aqua and right charts are for Terra. (a) and (b) Nighttime desert, (c) and (d) daytime desert, (e) and (f) nighttime ocean, and (g) and (h) daytime ocean.

to reduce the effect of scattering from neighboring pixels. In addition, this additional uniformity filtering also reduces the geomatching effect on the comparison.

Figure 3 shows the pixel number after the uniformity and clear sky filtering. The blue symbols are the pixel number for a day and the red lines denote a 30-day moving average to show the seasonal trend. The desert site is located at the south of the Himawari-8 suborbital point. However, the ocean site has large cloud impact and the number of days and the number pixels with uniformly clear sky is much lower than the number obtained from the desert site. Measurement uncertainty decreases by square root of number of samples. Therefore, the desert site can enhance the comparison accuracy. The nighttime desert observations show a strong seasonal variation for both Aqua and Terra MODIS. Since clear sky filtering has been applied, the pixel number also varies with season.

3.3 Correction and Comparison

When analyzing the MODIS–AHI comparison, a view angle dependence in the MODIS measurements was observed. The selected sites have a fixed view for AHI and its measurements used as reference do not affect MODIS view angle dependence. For the desert site, AHI measurements have a fixed view angle. The MODIS–AHI difference from both sites exhibit a MODIS view angle dependence. The view angle dependence is analyzed by using an empirical model for both sites. Figure 4 shows a flowchart for the MODIS intercomparison using AHI as bridge.

For each pair of matching bands, the AHI BT measurements and MODIS BT measurements as well as the cloud mask are processed for the selected area. Based on the AHI grid, MODIS BT and cloud mask are resampled. After clear sky and uniformity filtering, the pixel-to-pixel MODIS–AHI differences are calculated. The view angle dependence is corrected using the empirical model. The Terra–AHI and Aqua–AHI difference as well as their precision are assessed using statistical analysis. The Terra–Aqua difference is derived by using the double difference and its precision is estimated from a statistical analysis.
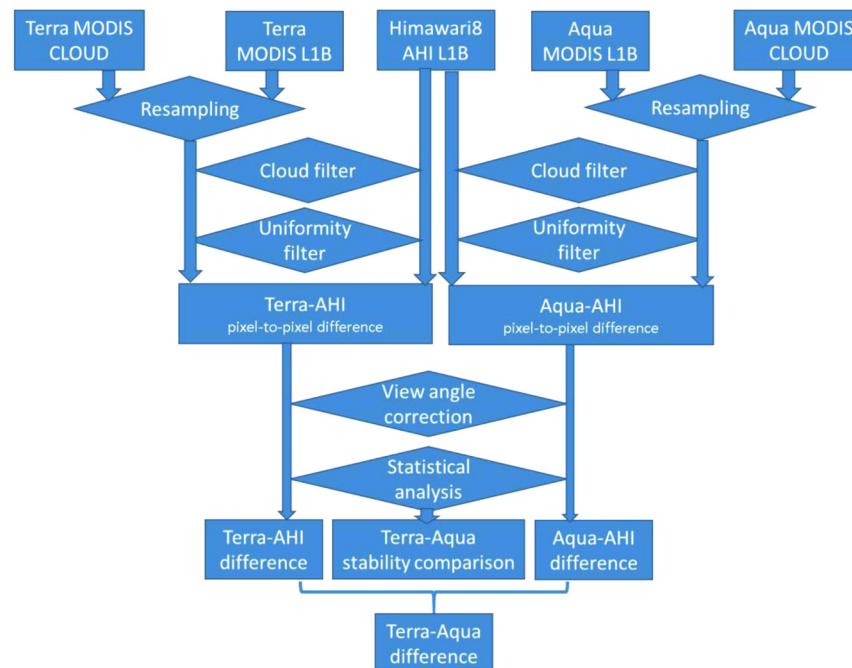
Fig. 4 Flowchart for the MODIS comparison using AHI as bridge and the processing for clear sky and uniformity filtering, view angle correction, and statistical analysis.

4 Comparison Results

4.1 *MODIS–AHI Difference*

In this work, the averaged comparisons from the year 2017 are analyzed. The 1-year averaging process will mitigate the impact due to seasonal fluctuations and also reduce the uncertainties associated with this comparison. The collocated L1B data with closest observation time for AHI and MODIS are collected and processed using the method described in Sec. 3. The differences between AHI and Aqua MODIS and between AHI and Terra MODIS are computed for all the spectrally matched bands. Figure 5 shows examples of the MODIS–AHI comparison for select bands using nighttime clear sky over the ocean site. Figure 6 shows examples of the MODIS–AHI comparison for selected bands over the desert site using nighttime clear sky observations. Bands 30 and 31 are selected to show on both Figs. 5 and 6. Band 31 is relatively stable for both Terra and Aqua MODIS and can be used as a reference. Band 30 shows the largest Terra–Aqua
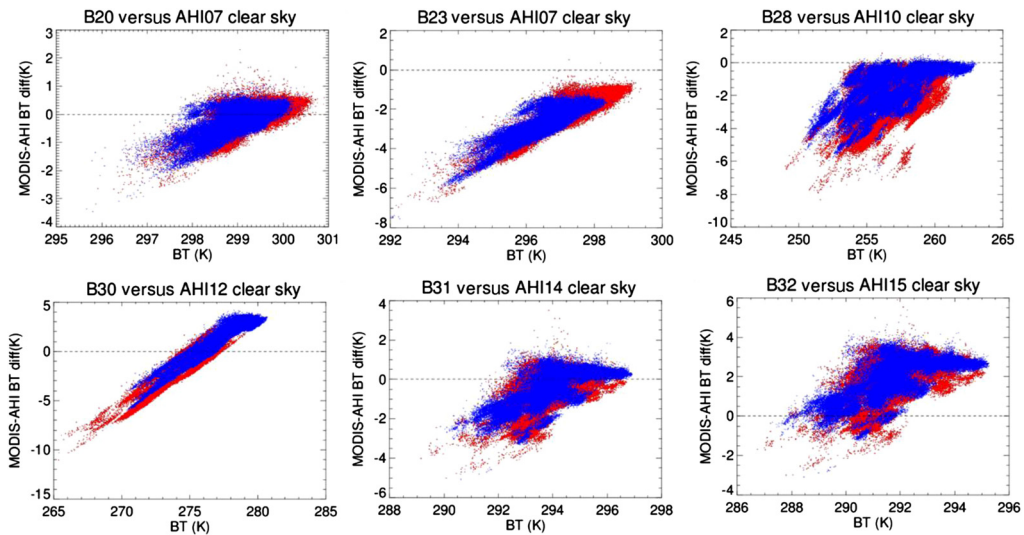

Fig. 5 The MODIS–AHI difference versus MODIS BT using the ocean site (nighttime clear sky) under AHI nadir. The red symbols are the Terra–AHI difference and blue symbols are Aqua–AHI difference.
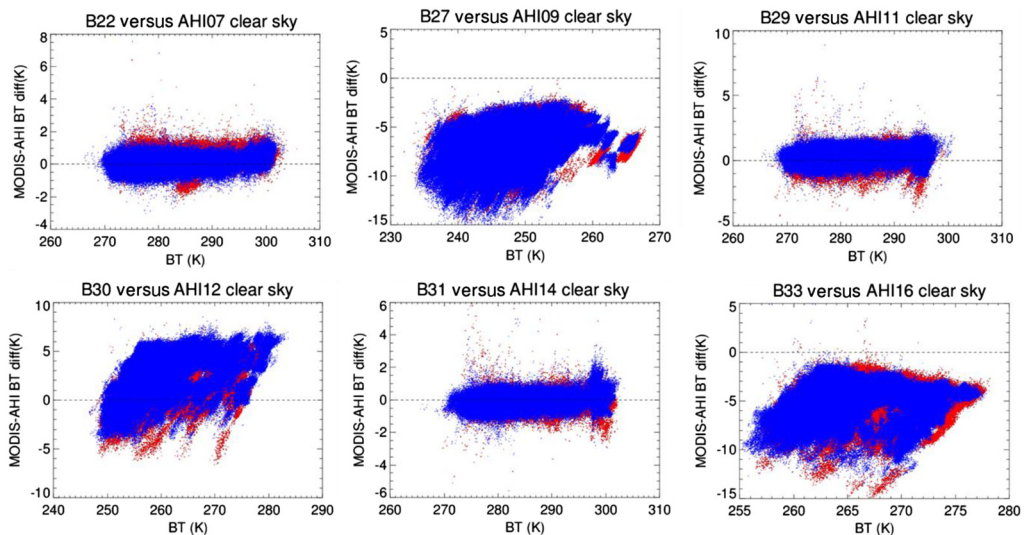

Fig. 6 The MODIS–AHI difference using the Strzelecki Desert site (nighttime clear sky). The red symbols are the Terra–AHI difference and blue symbols are Aqua–AHI difference.

difference for both sites. The significant spectral difference between the matched band pairs, as well as their calibration uncertainty, makes the MODIS–AHI difference scene and BT dependent. The dependence has been demonstrated using MODTRAN modeling for typical ocean and desert scenes along with the MODIS and AHI RSR shown in Fig. 1.

Since an entire year data are used, the scene temperature varies for all the bands. The ocean measurements have a narrow BT range while desert site has a larger BT range. As shown in Sec. 3.3, the desert site provides more clear sky samples. The MODIS–AHI difference covers a different range for each site. As mentioned in Sec. 3.3, the large MODIS–AHI difference includes a view angle effect that needs to be corrected. It also shows that the correction is band dependent.

4.2 *View Angle Dependency Correction*

The MODIS–AHI difference exhibits a MODIS view angle dependence for both ocean and desert sites. Even for a non-nadir desert site, the view angle dependence of AHI measurements is not an issue as it has the same bias for both Terra–AHI and Aqua–AHI differences. The bias is then removed in the double difference for the Terra–Aqua comparison. The view angle correction is empirically modeled and corrected to achieve an improved MODIS–AHI difference. Before applying the empirical model, the symmetry of the measurements on either side of nadir was verified. The symmetrical pattern is an indicator of the accuracy of the RVS for these bands. The daytime measurements do not exhibit the symmetrical feature (see discussion in Sec. 5.3) and are not included in the final results of comparisons.

After examining different models, an empirical model is selected to represent the view angle symmetry as

$$\Delta T = c_0 + c_1 (f - f_{\text{nadir}})^2 + c_2 (f - f_{\text{nadir}})^4, \tag{1}$$

where ΔT is the MODIS–AHI BT difference, f is the frame number along the scan direction, and f_{nadir} is the frame number corresponding to the nadir direction. The coefficients $c_{0,1,2}$ are fitting parameters. $(f - f_{\text{nadir}})$ is proportional to view angle.

The examples shown in Fig. 7 are the comparisons using the ocean site and in Fig. 8 using the desert site; the pink lines are the fitting for the Terra–AHI difference and green lines are the fitting for the Aqua–AHI difference. The coefficients $c_{0,1,2}$ derived from the regressions in
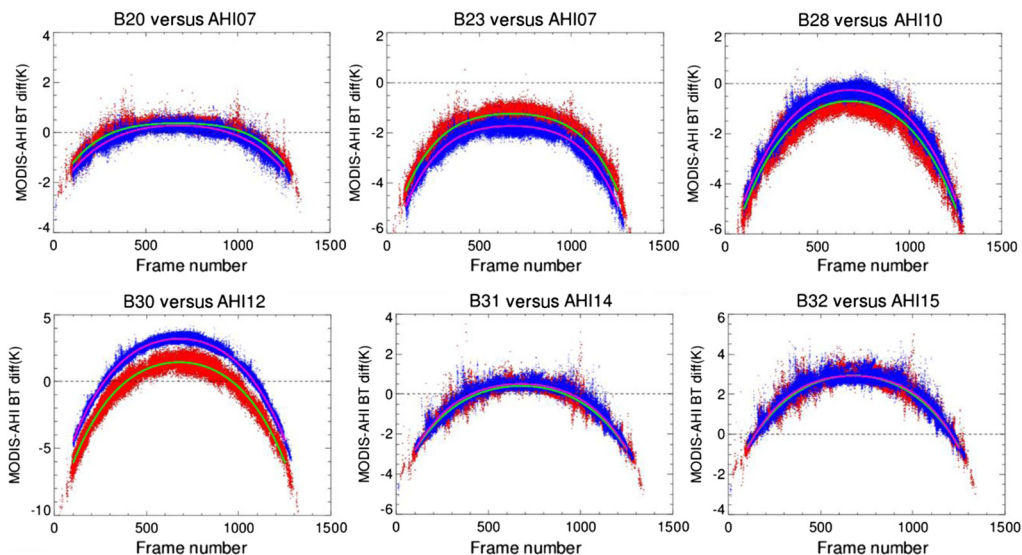

Fig. 7 The MODIS–AHI difference as a function MODIS frame number over the ocean site. The red symbols are the Terra–AHI difference and blue symbols are Aqua–AHI difference. The pink line is the fit using empirical model for Terra–AHI difference and green line is the fit for Aqua–AHI difference.

Fig. 8 The MODIS–AHI difference as a function MODIS frame number over the desert site. The red symbols are the Terra–AHI difference and blue symbols are Aqua–AHI difference. The pink line is the fit using empirical model for Terra–AHI difference and green line is the fit for Aqua–AHI difference.
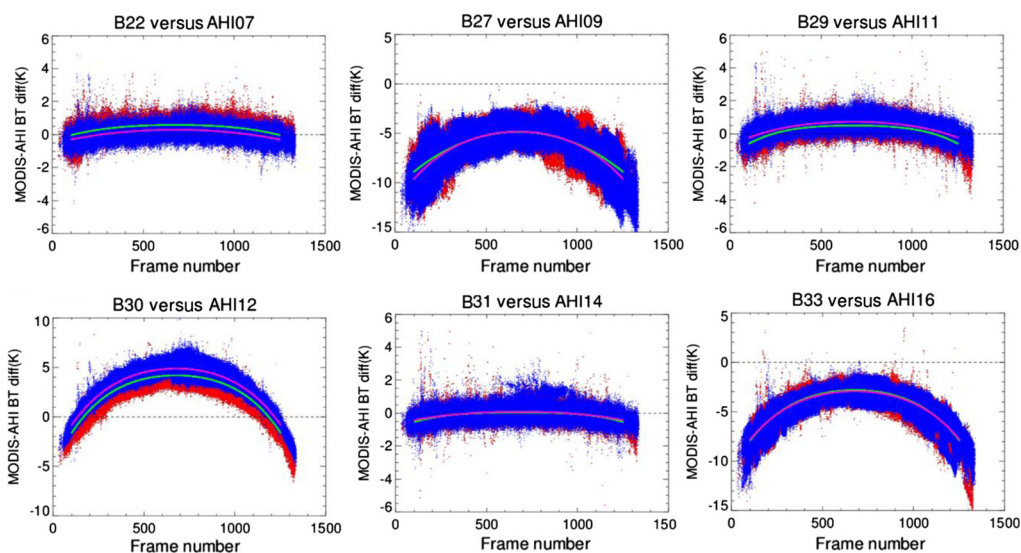
Figs. 7 and 8 are used to correct the view angle effect. The corrected MODIS–AHI difference as function MODIS frame number is shown in Fig. 9 for the ocean site and Fig. 10 for desert site. These view angle corrected MODIS–AHI differences are used to determine the Terra–Aqua difference.

The distribution of the MODIS–AHI difference over the desert site shows a larger range in comparison with the ocean site. There are two factors that may contribute to the increased distribution. The first is that the desert site has more clear-sky samples (pixels) covering a broader temperature range used for the comparison and the second is that the nonuniformity combined with geo-mismatching may also introduce larger noise. After correction, a residual view angle dependence is observed for some bands, for example, bands 27 and 33, especially for the desert site. For the desert site, the selected area is larger and some variations are present. The pixel matching in both location and size can introduce noise, especially for large view angles.
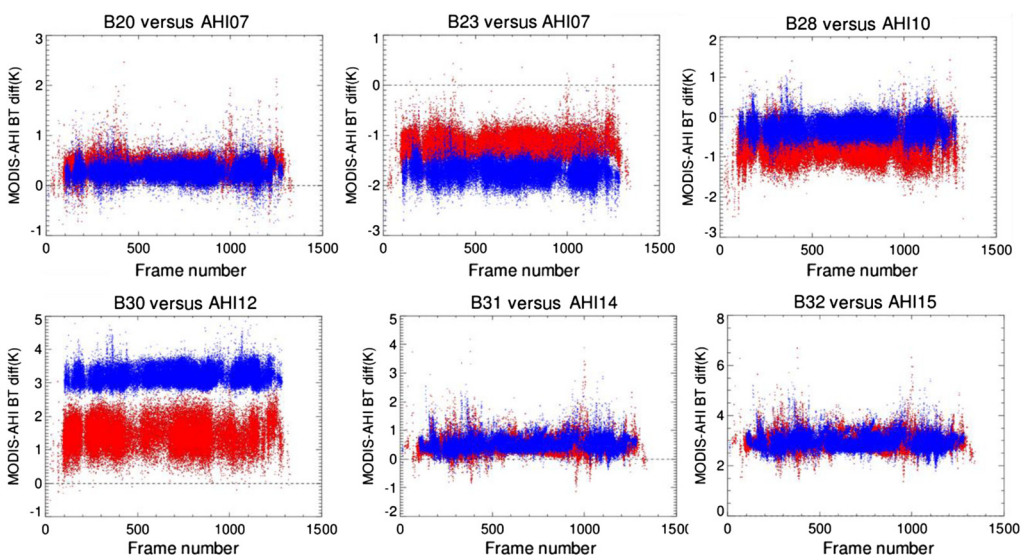

Fig. 9 The corrected MODIS–AHI difference as a function MODIS frame using the ocean site. The red symbols are the Terra–AHI difference and blue symbols are Aqua–AHI difference.
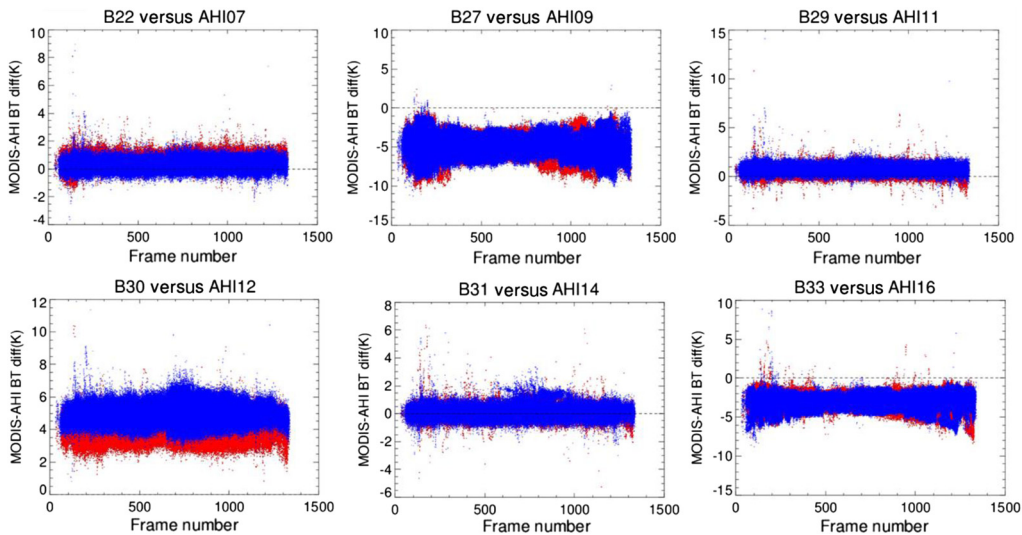
Fig. 10 The corrected MODIS–AHI difference as a function MODIS frame number for the desert site. The red symbols are the Terra–AHI difference and blue symbols are Aqua–AHI difference.

However, it contributes random noise and the impact on the comparison is largely reduced by using a large amount of samples.

4.3 Terra and Aqua Difference

As shown in Figs. 9 and 10, the comparison between AHI with Terra MODIS and AHI with Aqua MODIS shows distributions close to Gaussian for most bands. To assess the impact of this behavior on the comparison, the distribution is first quantified. Figures 11 and 12 show that the distribution over nighttime ocean and desert for select bands. The distribution is normalized to the peak count. The distribution of MODIS–AHI differences is very close to a Gaussian shape. The exception is band 27 over the desert site; the distribution is symmetrical but the shape does not follow a smooth Gaussian function. This may be related to the crosstalk issue and is discussed in Sec. 5.2.
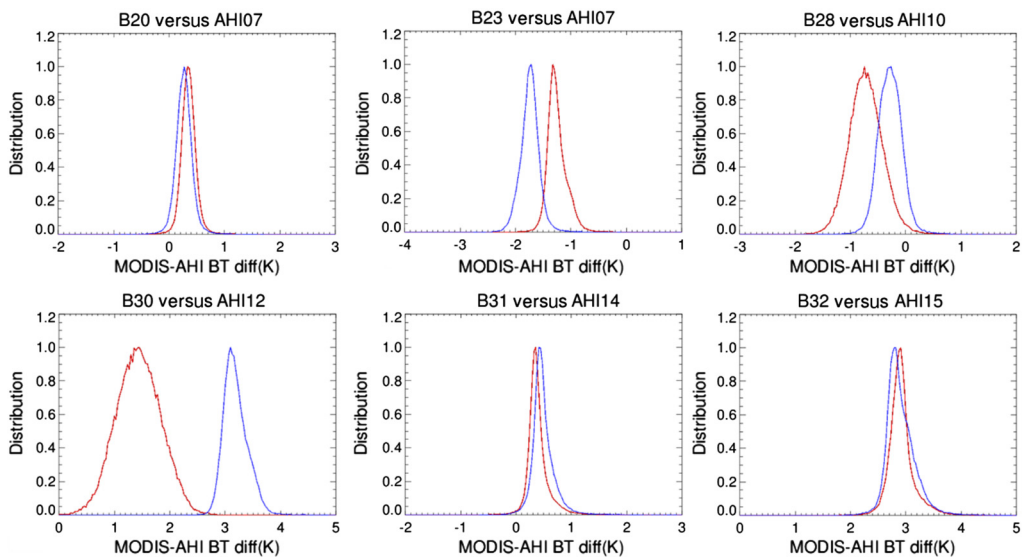

Fig. 11 The distribution of MODIS–AHI differences measured for selected bands over nighttime ocean. The red is for Terra–AHI difference and blue is for Aqua–AHI difference.
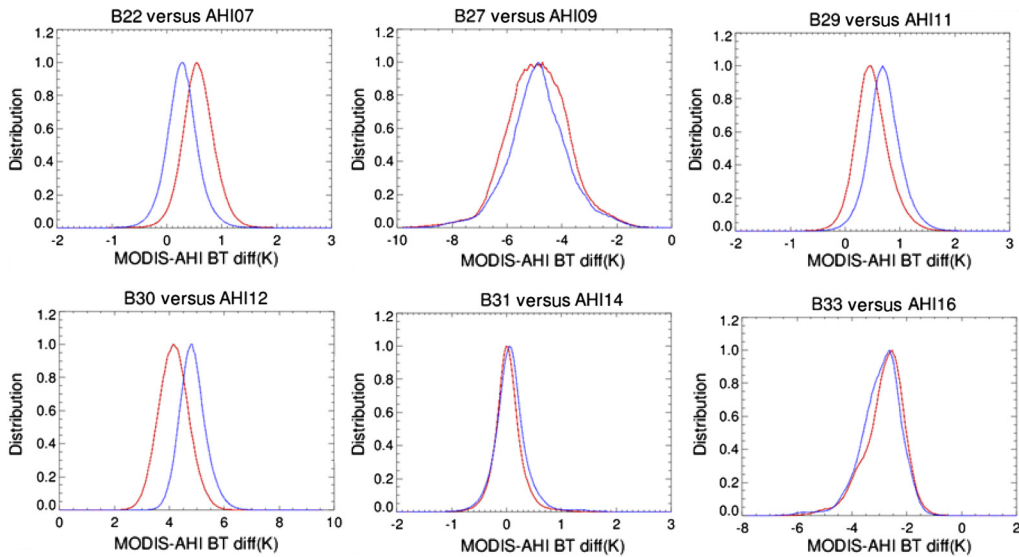
Fig. 12 The distribution of MODIS–AHI differences measured for selected bands over nighttime desert. The red is for Terra–AHI difference and blue is for Aqua–AHI difference. The distribution is normalized to the peak count.

A Gaussian profile is used to estimate the impact of these random effects. The Gaussian function is used as $A \exp\left[-\frac{(x-x_0)^2}{2\sigma^2}\right]$. When applying it to the distribution of MODIS–AHI differences, x is the scene BT, x_0 is the BT difference corresponding to the Gaussian peak, σ is the Gaussian width representing the uncertainty of the comparison, and A is the peak value before normalization. Two methods are used to derive the Terra–Aqua difference. The first method is to average the Terra–AHI differences and Aqua–AHI differences, respectively. Then the Terra–Aqua difference is derived using the double difference. The second method is to fit the Terra–AHI and Aqua–AHI differences to the Gaussian distribution and then take the difference between the two peaks.

Table 3 lists the Terra–Aqua difference for the different scenes from the two methods. The results from the two methods are consistent. The Terra–Aqua difference is up to 0.6 K except for bands 21 and 30. A linear calibration equation is used for band 21, widely used for fire detection. The uncertainty of its BT over oceans and deserts is larger than other bands. Band 30 has the largest difference and that difference is site dependent. Over the ocean, the difference is around 1.75 K, while over the desert, the difference is around 0.68 K. The large difference and scene dependence may be related to crosstalk.

Table 3 Terra–Aqua BT difference (K) for different scenes using the two methods.

	AHI	7	7	7	7	9	10	11	12	14	15	16
Scene	MODIS	20	21	22	23	27	28	29	30	31	32	33
Ocean	Average ocean BT	299.0	299.6	299.6	296.7	241.5	257.0	292.7	277.1	294.2	292.1	268.7
	Terra-Aqua Average	0.084	−0.320	0.348	0.489	0.554	−0.437	−0.378	−1.755	−0.095	0.089	0.282
	Peak	0.081	−0.370	0.332	0.447	0.450	−0.446	−0.341	−1.720	−0.095	0.033	0.285
Desert	Average desert BT	281.0	287.4	280.0	279.1	249.3	263.8	278.9	260.5	282.0	282.7	265.2
	Terra-Aqua Average	0.142	−0.881	0.293	0.307	−0.019	−0.286	−0.222	−0.689	−0.047	0.021	0.119
	Peak	0.146	−0.869	0.292	0.292	−0.008	−0.261	−0.235	−0.661	−0.041	−0.006	0.158

Table 4 MODIS–AHI comparison precision analysis. Terra extra noise using Aqua as reference. Exceptions are boldfaced indicating cases where Aqua has extra noise. In the calculation, more digits are used while the value in table is round to mK.

	AHI	7	7	7	7	9	10	11	12	14	15	16
Scene	MODIS	20	21	22	23	27	28	29	30	31	32	33
Ocean	$\sigma_{\text{Terra–AHI}}(K)$	0.11	0.38	0.15	0.13	0.72	0.29	0.22	0.41	0.10	0.14	0.28
	$\sigma_{\text{Aqua–AHI}}(K)$	0.13	0.64	0.11	0.14	0.64	0.20	0.18	0.20	0.12	0.19	0.23
	$\sigma_{\text{extra}}(K)$	**0.05**	**0.51**	0.10	0.05	0.32	0.21	0.13	0.36	0.07	**0.13**	0.16
Desert	$\sigma_{\text{Terra–AHI}}(K)$	0.26	0.61	0.27	0.56	1.06	0.29	0.28	0.55	0.19	0.42	0.62
	$\sigma_{\text{Aqua–AHI}}(K)$	0.28	0.54	0.25	0.66	0.92	0.26	0.27	0.45	0.22	0.44	0.66
	$\sigma_{\text{extra}}(K)$	**0.09**	0.29	0.09	**0.36**	0.52	0.12	0.08	0.32	**0.11**	**0.12**	**0.22**

4.4 Precision Comparison

The width of the distribution of MODIS–AHI difference includes uncertainties in the MODIS measurements, AHI measurements, and the comparison, as expressed as

$$\sigma^2_{\text{MODIS–AHI}} = \sigma^2_{\text{MODIS}} + \sigma^2_{\text{AHI}} + \sigma^2_{\text{comparison}}. \quad (2)$$

Since the same method is applied for both Terra–AHI and Aqua–AHI differences. The AHI measurement uncertainty and comparison method uncertainty, the second and third terms in Eq. (2), are almost the same for Terra–AHI and Aqua–AHI differences. Therefore, we can write

$$\sigma^2_{\text{Terra–AHI}} - \sigma^2_{\text{Aqua–AHI}} = \sigma^2_{\text{Terra}} - \sigma^2_{\text{Aqua}}. \quad (3)$$

The values of $\sigma^2_{\text{Terra–AHI}}$ and $\sigma^2_{\text{Aqua–AHI}}$ are derived from the Gaussian fits to the MODIS–AHI differences. For the precision comparison, if the MODIS with a smaller uncertainty is selected as a reference, the extra noise of the other MODIS is then estimated

$$\sigma_{\text{extra}} = \sqrt{|\sigma^2_{\text{Terra}} - \sigma^2_{\text{Aqua}}|}. \quad (4)$$

By applying Eq. (3), the extra noise can be derived using

$$\sigma_{\text{extra}} = \sqrt{|\sigma^2_{\text{Terra–AHI}} - \sigma^2_{\text{Aqua–AHI}}|}. \quad (5)$$

The extra noise, calculated using this equation for each band and scene, is listed in Table 4. For the majority of the comparisons, Aqua is the more stable. The bold indicates cases where Terra is considered more stable. The noise in the table is for a single measurement. More detailed discussion will be given in Sec. 5.4.

5 Discussions

The Terra–Aqua comparison shown may be impacted from some specific effects, such as spectral mismatching, scene effects, and Terra PV LWIR crosstalk. For these effects, it is challenging to quantify their impact. As a result, it is also challenging to quantify the uncertainty in the comparison results. In this section, potential impact from these effects and their uncertainty are discussed.
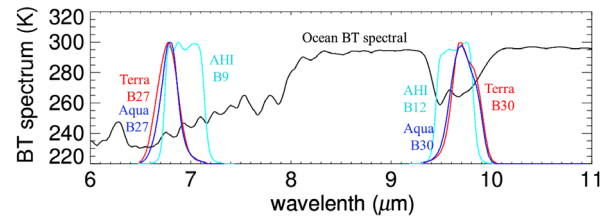
Fig. 13 The BT spectrum from MODTRAN modeling for a typical ocean site and the RSR for MODIS band 27 with AHI band 9 and MODIS band 30 with AHI band 12.

5.1 *Spectral Mismatching*

There are two kinds of spectral mismatching. One is between MODIS and AHI. Its effect on Terra–Aqua comparison is generally canceled using double difference method, which has been discussed in Sec. 2.3. The second is the spectral mismatch between the two MODIS instruments. Terra and Aqua MODIS were designed to have the same spectral bands. However, a slight difference between the RSR of these instruments exists and was characterized extensively during prelaunch testing. The radiometric calibration of the MODIS TEB use a detector-specific RSR characterized from prelaunch measurements. However, the BT measurement for certain scenes observed by the two instruments in different seasons will be impacted due to the RSR mismatch. The BT difference due to their RSR mismatch is estimated using the modeled radiance spectrum for each band for typical ocean and desert scenes using MODTRAN.[32]

Figure 13 shows the BT spectrum from MODTRAN modeling for a typical ocean site and the RSR for band 27 of two MODIS instruments with AHI band 9 and MODIS band 30 with AHI band 12. The RSR are from prelaunch tests and implemented in L1B BT calculations. Bands 27 and 30 have largest impact from the spectral mismatching. The spectral resolution in MODIS prelaunch tests is large and is different between Terra and Aqua. The large spectral resolution and their difference between Terra and Aqua, combined with large fluctuation and features of BT spectrum, can introduce uncertainty in the analysis of the spectral mismatching effect, especially for bands 27 and 30. In addition, the comparison in this analysis uses an entire year of measurements and these estimates from a typical scene are only for Ref. 33. Table 5 lists their difference from the modeling. For most bands, the impact is up to 0.3 K, except bands 27 and 30.

5.2 *Terra PV LWIR Crosstalk Impact*

Terra has a known electronic crosstalk issue for LWIR bands 27 to 30. The crosstalk correction has been applied to the Collection 6.1 L1B data which is used in this work.[24] The crosstalk coefficients are derived from scheduled lunar observation and are updated if the coefficients change beyond a certain limit. As shown in Table 4, Terra bands 27 to 30 have large bias and extra noise comparison with Aqua. It is known that the crosstalk has a large impact on Terra bands 27 and 30 calibration and L1B product. Due to the time delay, the uncertainty of the crosstalk coefficients, and fluctuations in the sending bands, some residual crosstalk effect can impact the L1B data.

Table 5 The impact of the RSR difference on the Terra and Aqua comparison over typical ocean and desert scenes using MODTRAN modeling results.

Band	20	21	22	23	27	28	29	30	31	32	33
Terra (μm)	3.788	3.992	3.972	4.057	6.765	7.337	8.524	9.730	11.014	12.028	13.361
Aqua (μm)	3.780	3.982	3.972	4.062	6.787	7.349	8.555	9.723	11.026	12.042	13.365
Ocean (K)	−0.202	−0.288	−0.028	0.302	−0.565	−0.036	−0.105	0.588	−0.015	0.014	−0.051
Desert (K)	−0.138	−0.254	−0.025	0.303	−0.563	−0.038	−0.120	0.632	−0.017	0.005	−0.058

Table 3 shows a larger Terra–Aqua difference for bands 27 and 30 than those of other bands, except band 23. The Terra–Aqua differences for these two bands also have larger scene dependences. These issues can be attributed to residual impacts of crosstalk postcorrection. In addition, the crosstalk effect will also have seasonal variations and, as a result, the width of the Gaussian distributions becomes larger. As shown in Table 4 for bands 27 to 30, Terra has extra noise in relation to Aqua, which is larger than other bands, except band 21 over desert. However, the distributions of Terra–AHI difference are symmetric and most of them are still nearly Gaussian, except band 27 which has a symmetric non-Gaussian shape over desert. The impact of the crosstalk effects is random and will increase the comparison uncertainty. By collecting large number of samples, these effects are reduced. The systematic effects are included in the Terra–Aqua difference for these bands, which are mostly scene dependent.

5.3 Scene Effects

For the assessment of TEB performance, the nighttime measurements have an advantage, especially for MWIR bands. The empirical model cannot be applied to the daytime MODIS–AHI difference as function of frame number. For comparison, Fig. 14 shows an example for band 22. The MODIS–AHI difference during nighttime is symmetric around the nadir frame and the empirical model for view angle dependence works reasonably well. The daytime measurement is not symmetric across frames and therefore cannot be corrected using the empirical modeling. In addition, the two MODIS instruments have different overpass times and the ground BT range is also different. For some bands, saturation affects the Terra–AHI and Aqua–AHI comparison differently.

The asymmetric pattern of the MODIS measurements in the daytime is more significant for MWIR bands than LWIR bands. As shown in Fig. 14 for band 22, a clear view angle-dependent pattern is observed in the daytime measurements in comparison with the nighttime measurements. One is the sun glint effect at certain view angle range over the ocean scene. The second is the asymmetric measurement over the two sides around the nadir. As presented in Ref. 34, the surface solar reflectance during daytime impacts the measurement in the MWIR bands.[34] The BT calculated from the radiance measurement includes the reflected solar radiance that is solar angle
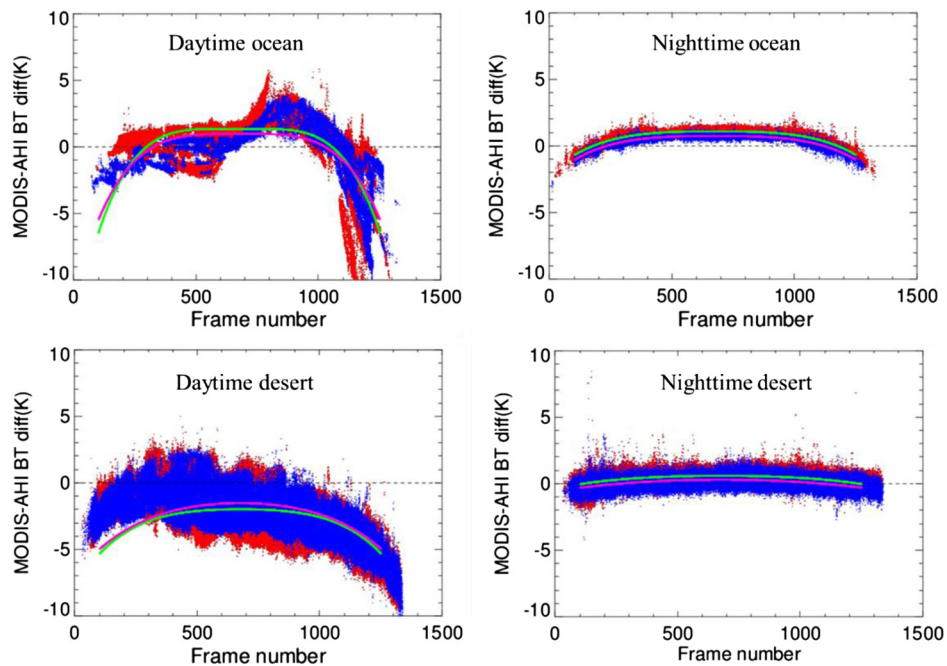

Fig. 14 The MODIS–AHI difference as function frame number for band 22 over daytime ocean, nighttime ocean, daytime desert, and nighttime desert. The red is for Terra–AHI difference and blue is for Aqua–AHI difference.

dependent. For the selected site, the view angle and the overpass time are closely related in the case of each MODIS instrument. The solar angle for one side of nadir is different than the other side. The retrieved radiance is different for the two sides. It causes an asymmetric pattern of the radiance measurements, as shown in Fig. 14 daytime measurement for both ocean and desert sites.

As shown in Figs. 7 and 8, the clear sky ocean scene under AHI nadir provides a narrower BT range than the desert scene. The BT dependence of the Terra–Aqua difference is reduced. However, this ocean site has much less clear sky pixels. This double comparison will be applied to cloudy pixels to analyze Terra–Aqua difference at low BT in our future work. On the other hand, the desert site has more clear sky pixels which enhanced the comparison accuracy. The desert site is located at the south of AHI nadir and has a fixed view angle. The desert site provides a larger range of ground BT and significantly more clear sky pixels for comparison.

5.4 Seasonal Variation

The seasonal variation is observed for MODIS–AHI difference and the comparison presented above is for the yearly averaged results. Figure 15 shows the daily averaged MODIS–AHI difference as function of day of the year, from clear sky nighttime desert site. Band 28 does not exhibit significant seasonal variation, whereas bands 29 and 31 show significant variation in the comparison. During the middle of the year, the MODIS–AHI difference shows more stable results. A significant seasonal variation is observed in the MODIS–AHI difference, as bands 23, 32, and 33. Both Terra–AHI difference and Aqua–AHI difference show the similar seasonal variation pattern for each band. Therefore, the seasonal variation impact on Terra–Aqua difference is small.

5.5 Comparison Uncertainty

The precision assessment in Sec. 4.4 is for one pixel-to-pixel comparison between instruments. The term precision is used to differentiate it from uncertainty. If the uncertainty is completely due to random effects, the uncertainty can be assessed using the width of the Gaussian distribution. In addition, the uncertainty of the mean of the measurements is the uncertainty of a single measurement divided by square root of the number of samples. Applying this to the MODIS–AHI comparison, the uncertainty of the average of N comparison samples is

$$\sigma_{\text{MODIS–AHI}}{}^{\text{Average}} = \frac{\sigma_{\text{MODIS–AHI}}}{\sqrt{N}}.$$ (6)
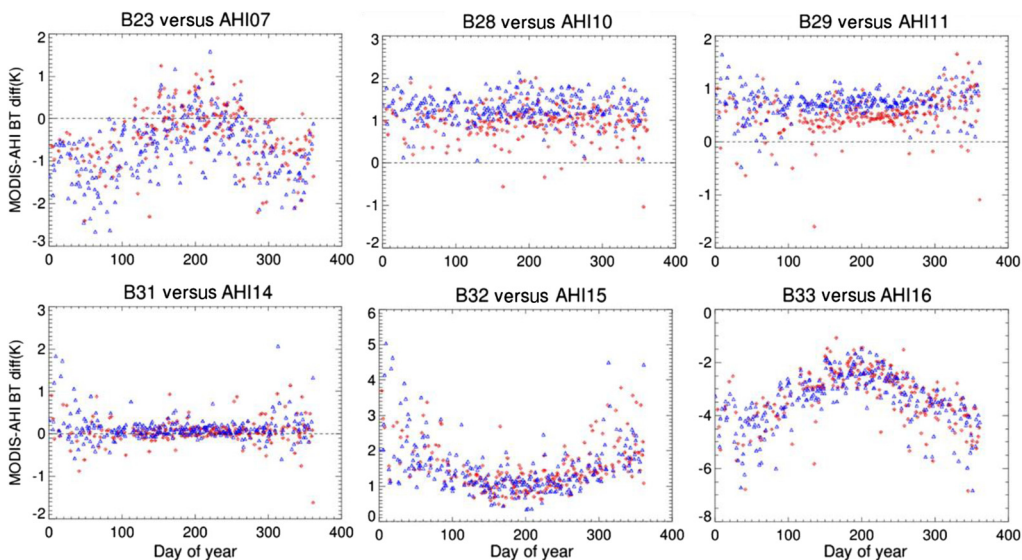

Fig. 15 The daily averaged MODIS–AHI difference as day of the year over nighttime desert. The red is for Terra–AHI difference and blue is for Aqua–AHI difference.

In this work, the entire year of data after resampling gives the around 12,000 samples for clear sky ocean and 55,000 samples for clear sky desert. As shown in Table 4, band 27 has the largest uncertainty of the Terra–AHI comparisons: 0.72 K for ocean and 1.06 K for desert. Averaging of large number of sample provides an improvement of 110 times for ocean and 230 times for desert. As a result, the uncertainty from the random effects is now on the order of mK. However, as discussed above, the uncertainty of MODIS–AHI difference should include the impact due to spectral mismatch, scene dependence, and crosstalk effects for some bands. In addition, both MODIS and AHI instrument calibrations use a quadratic function.[1,23] The impact of uncertainties of the calibration coefficients is BT dependent.[33] A BT-dependent comparison will be performed in our future analysis. For example, the desert scene has a relatively large BT range and the comparison can be assessed for various BT. In addition, totally cloudy scenes provide feasibility for the comparison over a low BT range.

6 Conclusion

The double difference method is applied to assess the differences in BT measurements between the two MODIS instruments using the geostationary imager, Himawari-8/AHI. Eleven TEBs on MODIS have spectrally overlapping bands with AHI. The sites selected are an ocean area around the Himawari-8 suborbital point and Strzelecki Desert located to the south of the Himawari-8 suborbital point. The time difference between the measurements from AHI and MODIS is <5 min. The methods of data resampling and double difference have been presented. The comparison is performed using year 2017 collection 6.1 L1B data from MODIS. A view-angle dependence has been observed in the MODIS–AHI difference. An empirical model is applied to remove this view angle dependence for both Terra and Aqua MODIS. The corrected MODIS–AHI differences are used for the comparison between Terra and Aqua using a double difference.

The PV LWIR bands 27 to 30 show relatively large Terra–Aqua differences and the differences are site dependent. In the case of band 30, over the ocean, the difference is around 1.76 K, while over the desert, the difference is around 0.69 K. Band 21 is low gain band for fire detection and its larger uncertainty is expected. The remaining bands show the Terra–Aqua difference up to 0.5 K. These large differences are likely due to residual crosstalk effects in the Terra PV LWIR bands 27 to 30. The calibration and LUT update procedure for Terra TEB has been improved based on assessments from these and other intercomparison results. The MODIS measurement precision is also compared using a Gaussian regression of the double difference. The impact of daytime measurements and the scene dependence have been discussed. The precision comparison is also very useful for the uncertainty assessment. For example, the PV LWIR bands have crosstalk penalty on their uncertainty. The comparison of measurement as well its precision can be used for future improvement of uncertainty assessment. The Terra–Aqua TEB comparison will be beneficial for MODIS calibration improvements which will enhance the L1B data quality. This method can also be applied to the comparison between SNPP/VIIRS and NOAA-20/VIIRS. Using an LEO sensor as a reference, such as MODIS or VIIRS, GEO-GEO comparisons, such as comparisons between ABI on board of NOAA-16/17 and AHI on Himawari, can also be performed.

References

1. X. Xiong et al., "Terra and Aqua MODIS thermal emissive bands on-orbit calibration and performance," *IEEE Trans. Geosci. Remote Sens.* **53**(10), 5709–5721 (2015).

2. X. Xiong et al., "15 years of Aqua MODIS on-orbit operation, calibration, and performance," in *IEEE Int. Geosci. and Remote Sens. Symp.*, pp. 4695–4698 (2017).

3. R. M. Cavalli, "Retrieval of sea surface temperature from MODIS data in coastal waters," *Sustainability* **9**(11), 2032 (2017).

4. J. A. Sobrino, J. El Kharraz, and Z. L. Li, "Surface temperature and water vapour retrieval from MODIS data," *Int. J. Remote Sens.* **24**, 5161–5182 (2003).

5. C. Moeller et al., "Improvements to Terra MODIS L1B, L2, and L3 science products through using crosstalk corrected L1B radiances," *Proc. SPIE* **10402**, 104020O (2017).

6. H. Yue et al., "The brightness temperature adjusted dust index: an improved approach to detect dust storms using MODIS imagery," *Int. J. Appl. Earth Obs. Geoinf.* **57**, 166–176 (2017).

7. S. Skakun et al., "Transitioning from MODIS to VIIRS: an analysis of inter-consistency of NDVI data sets for agricultural monitoring," *Int. J. Remote Sens.* **39**(4), 971–992 (2018).

8. P. Gupta et al., "Validation of MODIS 3 km land aerosol optical depth from NASA's EOS Terra and Aqua missions," *Atmos. Meas. Tech.* **11**(5), 3145–3159 (2018).

9. R. C. Levy et al., "The collection 6 MODIS aerosol products over land and ocean," *Atmos. Meas. Tech.* **6**, 2989–3034 (2013).

10. C. G. Hulley et al., "NASA's MODIS and VIIRS land surface temperature and emissivity products: a long-term and consistent earth system data record," *IEEE J. Sel. Topics Appl. Earth Obs. Remote Sens.* **11**(2), 522–535 (2018).

11. A. M. Toure et al., "Assimilation of MODIS snow cover fraction observations into the NASA catchment land surface model," *Remote Sens.* **10**(2), 316 (2018).

12. X. Xiong, C. Cao, and G. Chander, "An overview of sensor calibration inter-comparison and applications," *Front. Earth Sci. Chin.* **4**(2), 237–252 (2010).

13. G. Chander et al., "Overview of intercalibration of satellite instruments," *IEEE Trans. Geosci. Remote Sens.* **51**(3), 1056–1080 (2013).

14. C. Cao, M. Weinreb, and H. Xu, "Predicting simultaneous nadir overpasses among polar-orbiting meteorological satellites for intersatellite calibration of radiometers," *J. Atmos. Oceanic Technol.* **21**, 537–542 (2004).

15. X. Xiong, A. Wu, and C. Cao, "On-orbit calibration and inter-comparison of Terra and Aqua MODIS surface temperature spectral bands," *Int. J. Remote Sens.* **29**, 5347–5359 (2008).

16. A. Shrestha et al., "Evaluating calibration consistency of Terra and Aqua MODIS LWIR PV bands using Dome C," *Proc. SPIE* **10644**, 106440N (2018).

17. A. Shrestha, A. Angal, and X. Xiong, "Evaluation of MODIS and Sentinel-3 SLSTR thermal emissive bands calibration consistency using Dome C," *Proc. SPIE* **10644**, 106441U (2018).

18. S. Madhavan et al., "Evaluation of VIIRS and MODIS thermal emissive band calibration consistency using Dome C," *Proc. SPIE* **9639**, 963913 (2015).

19. H. J. Simon, R. G. V. H. Tonooka, and S. G. Schladow, "Absolute radiometric in-flight validation of mid infrared and thermal infrared data from ASTER and MODIS on the Terra spacecraft using the Lake Tahoe, CA/NV, USA, automated validation site," *IEEE Trans. Geosci. Remote Sens.* **45**(6), 1798–1807 (2007).

20. D. C. Tobin et al., "Use of Atmospheric Infrared Sounder high-spectral resolution spectra to assess the calibration of moderate resolution imaging spectroradiometer on EOS Aqua," *J. Geophys. Res. Atmos.* **111**, D09S05 (2006).

21. C. Moeller, W. P. Menzel, and G. Quinn, "Review of Terra MODIS thermal emissive band L1B radiometric performance," *Proc. SPIE* **9218**, 92180T (2014).

22. P. Veglio et al., "Long-term assessment of Aqua MODIS radiance observation using comparisons with AIRS and IASI," *J. Geophys. Res. Atmos.* **121**, 8460–8471 (2016).

23. X. Xiong et al., "MODIS on-orbit calibration and characterization," *Metrologia* **40**, S89–S92 (2003).

24. T. Wilson et al., "Development and implementation of an electronic crosstalk correction for bands 27-30 in Terra MODIS collection 6," *Remote Sens.* **9**(6), 569 (2017).

25. K. Bessho et al., "An introduction to Himawari-8/9 Japans new-generation geostationary meteorological satellites," *J. Meteorol. Soc. Jpn. Ser. II* **94**(2), 151–183 (2016).

26. T. J. Schmit et al., "A closer look at the ABI on the GOES-R series," *Bull. Am. Meteorol. Soc.* **98**(4), 681–698 (2017).
27. P. Griffith, "Advanced Himawari Imager (AHI) design and operational flexibility," in *6th Asia/Oceania Meteorol. Satellite Users' Conf.*, (2015).
28. A. Okuyama et al., "Preliminary validation of Himawari-8/AHI navigation and calibration," in *6th Asia/Oceania Meteorol. Satellite Users' Conf.*, (2015).
29. P. M. Teillet et al., "Prime candidate earth targets for the post-launch radiometric calibration of space-based optical imaging instruments," *Proc. SPIE* **6677**, 66770S (2007).
30. R. M. Mitchell et al., "Selection and initial characterization of a bright calibration site in the Strzelecki Desert, South Australia," *Can. J. Remote Sens.* **23**(4), 342–353 (1997).
31. S. Platnick et al., "The MODIS cloud products: algorithms and examples from Terra," *IEEE Trans. Geosci. Remote Sens.* **41**(2), 459–473 (2003).
32. A. Berk et al., *MODTRAN 5.2.0.0 User's Manual*, Air Force Research Laboratory, Space Vehicles Directorate, Air Force Materiel Command, Bedford, Massachusetts, 01731–3010 (2008).
33. T. Chang and X. Xiong, "Assessment of MODIS thermal emissive bands on-orbit calibration," *IEEE Trans. Geosci. Remote Sens.* **49**(6), 2415–2425 (2011).
34. F. Petitcolin and E. Vermote, "Land surface reflectance, emissivity and temperature from MODIS middle and thermal infrared data," *Remote Sens. Environ.* **83**(1-2), 112–134 (2002).

Tiejun Chang received his MS degree in computer science from Montana State University and his PhD in optics from University of Paris-Sud, France. Currently, he is a lead optical engineer with Science Systems and Applications, Inc., Lanham, Maryland. His work focuses on radiometric calibration and validation of satellite remote sensor and has experience on prelaunch test and on-orbit calibration for MODIS, VIIRS, AVHRR, and GOES-R/ABI. He is working with MODIS Characterization and Support Team (MCST) and VIIRS Characterization and Support Team (VCST) at the National Aeronautics and Space Administration (NASA), Goddard Space Flight Center (GSFC).

Xiaoxiong Xiong received his BS degree in optical engineering from the Beijing Institute of Technology, Beijing, China, and his PhD in physics from the University of Maryland, College Park. He is an optical physicist at the National Aeronautics and Space Administration (NASA), Goddard Space Flight Center (GSFC), currently serving as the MODIS project scientist and the technical lead for both the MODIS Characterization Support Team (MCST) and the VIIRS Characterization Support Team (VCST). Before joining the NASA/GSFC, he had also worked in the fields of optical instrumentation, nonlinear optics, laser and atomic spectroscopy, resonance ionization mass spectrometry at universities, industry, and the National Institute of Standards and Technology (NIST).

Amit Angal received his MS degree in electrical engineering from South Dakota State University, Brookings, South Dakota, USA. Currently, he is a lead optical engineer and a supervisor with Science Systems and Applications, Inc., Lanham, Maryland, USA, where he is involved in the radiometric characterization and calibration of remote sensing instruments. He is primarily involved in the on-orbit calibration of the reflective solar bands of the Moderate-Resolution Imaging Spectroradiometer (MODIS) instruments on board the terra and aqua spacecraft. He has also supported the CLARREO Mission Preformulation activities in the reflective solar spectrum. In addition, he supports the preflight calibration of the JPSS-2 VIIRS instrument and is involved with the early on-orbit calibration and validation of the JPSS-1VIIRS instrument. His research interests include cross-calibration between Landsat and MODIS instruments.